

# Citrus black spot detection using hyperspectral imaging

Daegwan Kim<sup>1</sup>, Thomas F. Burks<sup>2\*</sup>, Mark A. Ritenour<sup>3</sup>, Jianwei Qin<sup>4</sup>

(1. *Asan Institute for Life Sciences, Asan Medical Center, Songpa-gu, Seoul 138-736, Korea;*

2. *Department of Agricultural & Biological Engineering, University of Florida, Gainesville, FL 32611, USA;*

3. *Indian River Research and Education Center (IRREC), University of Florida, Ft. Pierce, FL 34945, USA;*

4. *Environmental Microbial and Food Safety Laboratory (EMFSL), Agricultural Research Service,*

*U.S. Department of Agriculture, Beltsville, MD 20705, USA)*

**Abstract:** This paper describes the development of a hyperspectral imaging approach for identifying fruits infected with citrus black spot (CBS). Hyperspectral images were taken of healthy fruit and those with CBS symptoms or other potentially confounding peel conditions such as greasy spot, wind scar, or melanose. Spectral angle mapper (SAM) and spectral information divergence (SID) hyperspectral analysis approaches were used to classify fruit samples into two classes: CBS or non-CBS. The classification accuracy for CBS with SAM approach was 97.90%, and 97.14% with SID. The combination of hyperspectral images and two classification approaches (SID and SAM) have proven to be effective in recognizing CBS in the presence of other potentially confounding fruit peel conditions. The study result can be a reference for the non-destructive detection of fruits infected with citrus black spot.

**Keywords:** citrus black spot, hyperspectral imaging, spectral angle mapper, spectral information divergence, imaging processing

**DOI:** 10.3965/ijabe.20140706.004

**Citation:** Kim D, Burks T F, Ritenour M A, Qin J W. Citrus black spot detection using hyperspectral imaging. *Int J Agric & Biol Eng*, 2014; 7(6): 20–27.

## 1 Introduction

Once citrus trees are infected with CBS, their fruit yield and visual quality are greatly reduced and fruits with CBS symptoms are not acceptable in some important fresh fruit export markets, such as those of the European Union<sup>[1]</sup>. Therefore, it is important to control this disease in the field to preserve profitable production and to detect and eliminate infected fruit at the packinghouse to maintain marketability.

CBS symptoms can be quite variable and are identified by cosmetic lesions on the fruit peel<sup>[2]</sup>. CBS hard spot lesions, the most common symptom type, begin as small orange or red spots with black margins that enlarge and become necrotic. Other symptoms of CBS on citrus fruit peel include virulent spot, cracked spot, and false melanose<sup>[3]</sup>. Detecting fruits infected with CBS can also help in controlling the spread of this disease to areas that are currently free of CBS. The design and implementation of technologies that can efficiently detect CBS disease will greatly aid in the control effort.

The identification of various crops and plant using machine vision and image processing techniques has been studied by numerous researchers. Jimenez et al.<sup>[4]</sup> surveyed several computer vision approaches for locating fruit in trees for robotic harvesting. Regunathan and Lee<sup>[5]</sup> identified fruit count and size using machine vision and an ultrasonic sensor. Burks et al.<sup>[6]</sup> developed a method for classifying weed species using color texture

**Received date:** 2014-11-23    **Accepted date:** 2014-12-02

**Biographies:** **Daegwan Kim, PhD**, Graduate Student, research interests: hyperspectral imaging. Email: [dgkim0306@gmail.com](mailto:dgkim0306@gmail.com). **Mark A. Ritenour, PhD**, Professor, research interests: post harvest technology. Email: [ritenour@ufl.edu](mailto:ritenour@ufl.edu). **Jianwei Qin, PhD**, Postdoctoral Research Associate, research interests: optical sensing and control. Email: [jianwei.qin@ars.usda.gov](mailto:jianwei.qin@ars.usda.gov).

\* **Corresponding author: Thomas F. Burks, PhD**, Professor, research interests: robotics and machine vision. Mailing address: 1740 Museum Rd, POB 110570, Gainesville, FL 32606. Email: [tburks@ufl.edu](mailto:tburks@ufl.edu). Tel.: +1-352-392 1864; Fax: +1-352-392-4092

features and discriminant analysis. Tang et al.<sup>[7]</sup> presented gabor wavelets and neural networks algorithms to develop a texture-based weed classification method. Pydipati et al.<sup>[8]</sup> identified citrus disease using the co-occurrence matrix method, (CCM) texture feature method and discriminant analysis. Du et al.<sup>[9]</sup> described five different texture feature methods, including the common first-order gray-level statistics (FGLS), run length matrix (RLM), gray-level co-occurrence matrix (GLCM), fractal dimension (FD), and wavelet transform (WT) based methods.

In recent years, optical techniques have been used widely in the food processing and inspection application. In particular, hyperspectral imaging technologies have had growing interest for use in quality and safety inspection of food and agricultural products<sup>[10]</sup>. Previous research has demonstrated hyperspectral imaging technologies and applications for agricultural products. Jiang et al.<sup>[11]</sup> used hyperspectral fluorescence imaging to analyze the differences between walnut shells and meat. A hyperspectral fluorescence imaging system scanned samples at 79 different wavelengths ranging from 425 nm to 775 nm with 4.5 nm increments, later data redundancy was reduced through principal component analysis (PCA). Zhang et al.<sup>[12]</sup> suggested a novel classification approach for distinguishing healthy and fungal infected wheat kernels during storage. The research showed the potential use of NIR hyperspectral imaging in grain quality assessment. The research used NIR hyperspectral imaging and support vector machine (SVM) for identifying the fungi that caused the infection. Kim et al.<sup>[13]</sup> researched a method for using hyperspectral data to identify wavebands to be used in multispectral detection systems, and evaluated spatial and spectral responses of hyperspectral reflectance images of fecal contaminated apples. Lee et al.<sup>[14]</sup> used the hyperspectral imaging technique to detect defects on apple peel after harvest using a wavelength selection method.

In hyperspectral image classification approaches, a spectral angle mapper (SAM) and spectral information divergence (SID) classification that measures the spectral similarity between two spectra has been applied to various agricultural products and systems. Park et al.<sup>[15]</sup>

used SAM algorithms to detect fecal and ingesta contaminants on the surface of poultry carcasses. Qin et al.<sup>[16]</sup> introduced the detection of citrus canker using SID classification methods. Yang et al.<sup>[17]</sup> used the SAM method on airborne hyperspectral imagery for mapping yield variability.

This paper reports on work to develop a hyperspectral-based machine vision system for detecting and distinguishing fruit CBS symptoms from other common citrus peel conditions. This approach could be used in an off-line fruit blemish detection system, or could be used as the basis for the development of a real-time multi-spectral detection system. The overall objective of this research was to develop and compare the performance of two hyperspectral classification methods, spectral angle mapper (SAM) and spectral information divergence (SID), for detection of CBS using a hyperspectral imaging system.

## 2 Materials and methods

### 2.1 Fruit sample collection

'Valencia' oranges were hand-picked from citrus groves near Ft. Pierce in southeastern Florida in Apr. 2010. The fruit samples included marketable fruit and those with symptoms of CBS, greasy spot, melanose, and wind scar for a total of 525 samples. Representative images for each peel condition are shown in Figure 1. All fruit samples were washed with a mild soap to remove surface dirt before imaging. To maximize the number of hyperspectral images collected from the limited number of CBS samples, three faces of each fruit (with 120 °rotation intervals) were collected.

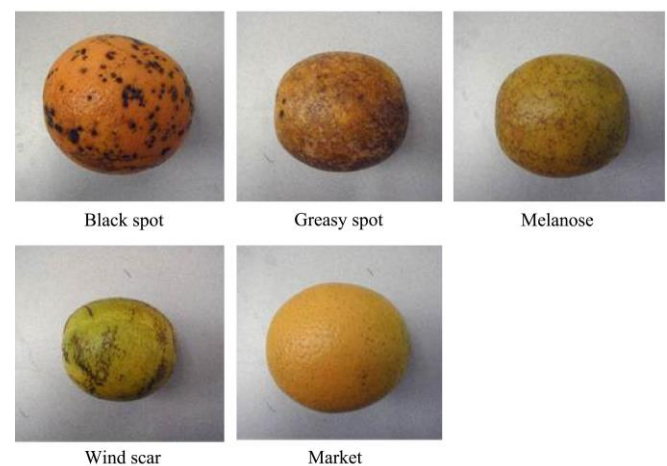


Figure 1 Representative images for each peel condition

## 2.2 Hyperspectral image acquisition

A hyperspectral line-scan imaging system, as shown in Figure 2, was used for acquiring hyperspectral images of the fruit samples.

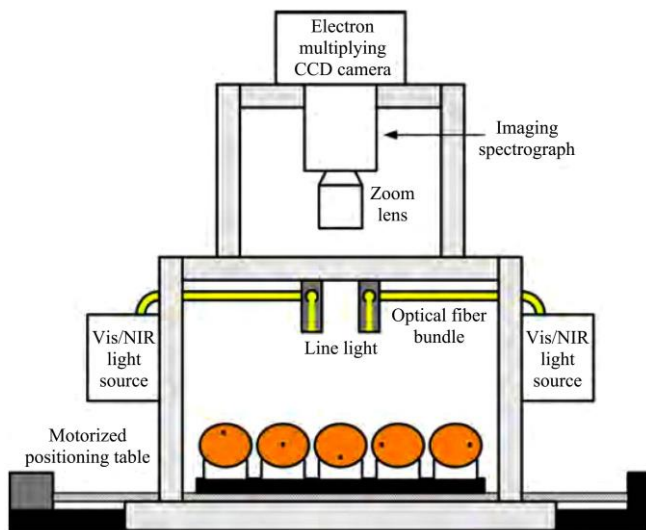


Figure 2 Hyperspectral line-scan imaging system

This system was based on design recommendations by Kim et al. [13]. The imaging system consisted of an electron-multiplying charge-coupled-device (EMCCD) camera (Luca, Andor Technology Inc., South Windsor, CT) with imaging spectrograph (ImSpector V10E, Spectral Imaging Ltd., Oulu, Finland) and a C-mount lens (Rainbow CCTV S6X11, International Space Optics, S.A., Irvine, CA), a pair of halogen line lamps (21 V, 150 W) powered with a DC voltage regulated power supply (Dolan-Jenner Industries, Inc., Lawrence, MA). This equipment was placed inside a dark box to eliminate undesirable external light. The reflectance light source consisted of two 21 V, 150 W halogen lamps powered with a DC voltage regulated power supply (Techni Quip, Danville, CA). The light was transmitted through optical fiber bundles toward line light distributors. Two line lights were arranged to illuminate the Image Field of View (IFOV).

The EMCCD has  $1004 \times 1002$  pixels and a double-stage Peltier device to cool to  $-80^\circ\text{C}$ . A programmable, motorized positioning table (BiSlide-MN10, Velmex Inc., Bloomfield, NY) moved citrus samples (five for each run) transversely through the line of the IFOV. For five fruit samples 1 740 line scans were performed, and 400 pixels covering the scene of the fruit at each scan were saved, generating a 3-D hyperspectral image cube with the

spatial dimension of  $1740 \times 400$  for each band.

The hyperspectral imaging software to transfer data and parameterization was developed using the Andor Software Development Kit (SDK, Luca, Andor Technology Inc.) for the hyperspectral line scan imaging system. An Hg-Ne spectral calibration lamp (Oriel Instruments, Stratford, CT) was used to investigate spectral calibration of the system. Because of low light output in the visible region less than 450 nm, and low quantum efficiency of the EMCCD in the NIR region beyond 930 nm, the wavelength range between 451.67 and 927.71 nm was used (totaling 92 bands with a spectral resolution of 5.2 nm).

## 2.3 Flat-field corrected images

Flat-field corrections were performed on the hyperspectral images to obtain the relative reflectance prior to image analysis and image processing for classification. Equation (1) was used for the flat-field correction to obtain the relative reflectance  $R$  for the 92 spectral bands. Flat-field correction technique can reduce uneven illumination and distortion.

$$R(w) = \frac{R_{sample}(w) - R_{dark}(w)}{R_{white}(w) - R_{dark}(w)} \times r \quad (1)$$

where,  $R(w)$  is the relative reflectance;  $R_{sample}(w)$  is the original sample image with the CCD values ranging between 0–16383 (14-bit EMCCD);  $R_{white}(w)$  is the reference image acquired from the white spectralon calibration panel;  $R_{dark}(w)$  is the dark current image obtained with a cap covering the camera lens;  $w$  is the wavelength;  $r$  is the reflectance factor of the calibration panel.

The actual reflectance factor for the white spectralon panel is about 99% in the wavelength range measured by the hyperspectral imaging system, however a reflectance factor of 100% was used in this study for simplicity. The relative reflectance  $R(w)$ , which has a value between 0 and 1, was then scaled to a range of 0 to 10 000 to increase the dynamic range of the adjusted reflectance.

To reduce image noise and processing time, the fruit peel area was separated from the background by creating a fruit parameter mask. The mask was created, by manual inspection, using a threshold value determined from the hyperspectral image which gave the largest contrast between the fruit and background. After

masking the background, the size of image was reduced by half by resampling which yielded equivalent spatial resolution in the horizontal and vertical dimensions. The resulting pre-processed images then became the test samples to be used in classification studies to validate the performance of SID and SAM algorithms for identifying CBS conditions on fruit.

#### 2.4 Hyperspectral image analysis and classification

The spectral angle mapper (SAM) and spectral information divergence (SID) algorithms are two important supervised classification methods used in analyzing the spectral characteristics of agricultural products. They are described in the following section.

#### 2.5 Spectral angle mapper

The main concept of SAM is to calculate the angle between endmember spectra and target spectra as vectors in a space with dimensionality equal to the number of bands (Yang et al.<sup>[18]</sup>). The formula of spectral angle ( $\theta$ ) is calculated as:

$$\theta = \cos^{-1} \left( \frac{\sum_{\lambda=1}^M \rho_{\lambda} \rho'_{\lambda}}{L_{\rho} L_{\rho'}} \right) \quad (2)$$

where,  $M$  is the number of spectral bands;  $\rho_{\lambda}$  is the reflectance of endmember spectrum;  $\rho'_{\lambda}$  is the reflectance of a target spectrum;  $L_{\rho}$  is the length of the endmember vector;  $L_{\rho'}$  is the length of the target spectrum vector.

The length of the endmember vector and the target spectrum vector are calculated as:

$$L_{\rho} = \sqrt{\sum_{\lambda=1}^M \rho_{\lambda}^2}, \quad L_{\rho'} = \sqrt{\sum_{\lambda=1}^M \rho'_{\lambda}{}^2} \quad (3)$$

After the spectral angle ( $\theta$ ) is found, it is then compared with a threshold value if the threshold is below the angle, the target spectrum is determined as classifying to the end member class.<sup>[18]</sup>

#### 2.6 Spectral Information Divergence

While SAM is a deterministic method, SID is a probabilistic method that allows for variations in pixel measurements, where probability is measured from zero to a user-defined threshold<sup>[19]</sup>. Chang<sup>[20]</sup> described the derivation of SID.

The hyperspectral pixel vector is given by

$$X = (x_1, x_2, x_3, \dots, x_n, \dots, x_N)^T \quad (4)$$

Each component  $x$  can be modeled as a random variable by defining an appropriate probability distribution. Due to the nature of reflectance, assume that all components  $x_n$ 's in  $X$  are non-negative. Thus, the probability measure can be defined as:

$$p_j = \frac{x_j}{\sum_{n=1}^N x_n} \quad (5)$$

and the desired probability vector is

$$P = \{p_l\}_{l=1}^L \quad (6)$$

Assume that

$$Y = (y_1, y_2, y_3, \dots, y_n, \dots, y_N)^T \quad (7)$$

is another pixel with the probability distribution given by

$$Q = \{q_l\}_{l=1}^L \text{ and } q_j = \frac{x_j}{\sum_{n=1}^N y_n} \quad (8)$$

Thus, spectral information divergence (SID) can be given by:

$$SID(X, Y) = D(X \parallel Y) + D(Y \parallel X) \quad (9)$$

where,  $(X \parallel Y)$ , called as the relative entropy of  $Y$  with respect to  $X$ , is defined by

$$\begin{aligned} D(X \parallel Y) &= \sum_{l=1}^L p_l \log \left( \frac{p_l}{q_l} \right) \text{ and } D(Y \parallel X) \\ &= \sum_{l=1}^L q_l \log \left( \frac{q_l}{p_l} \right) \end{aligned} \quad (10)$$

Therefore, the value of SID shows the use of the relative entropy and the similarity between two spectral pixels.

#### 2.7 Black spot classification

A detailed flowchart illustrating the SAM and SID classification algorithms is shown in Figure 3.

In this study, the mean reflectance spectra from  $3 \times 3$  pixel regions of interest (ROIs) from 10 CBS sample regions were used for describing endmember spectra to extract statistics data for classification. The ROIs were randomly selected from CBS infected image samples by manually selecting the  $3 \times 3$  window inside the boundary of a CBS lesion. Since the endmember spectra was composed of the mean of the actual 10 CBS samples, it created a unique endmember, thus allowing the original 10 CBS samples to be returned to the data set and used for testing. After applying SID and SAM mappings to the hyperspectral image of each test sample, rule images

were used to separate CBS lesions from other fruit peel conditions.

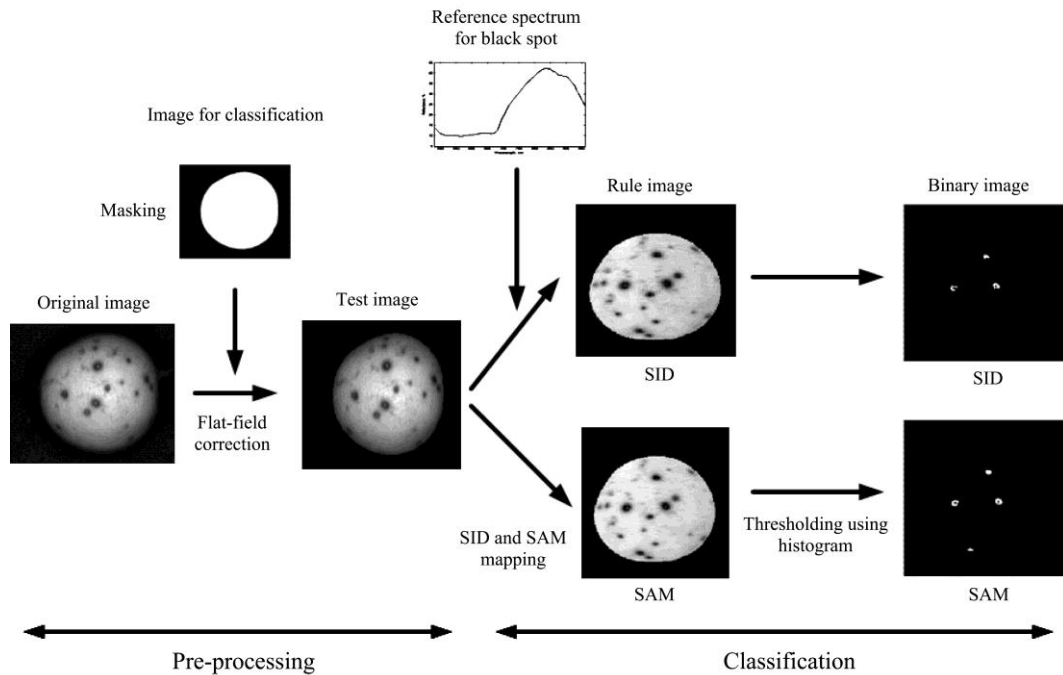


Figure 3 A detailed illustration of SAM and SID classification algorithms

### 3 Results and analyses

#### 3.1 Spectral characteristics of black spot and other conditions

The reflectance spectra of the various peel conditions (CBS, market quality and other diseases) over the wavelength range from 483 nm to 959 nm are shown in Figure 4. These plots were developed using the mean of 10 CBS spectra from different hyperspectral image samples. The spectra of each peel condition shows a similar pattern, regardless of the surface, with the difference appearing as shifts either upward or downward depending on the peel conditions reflectance characteristics.

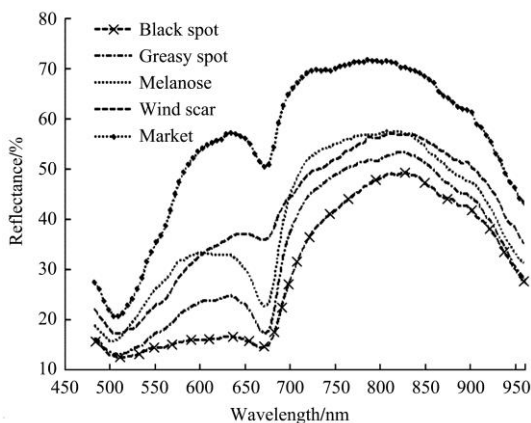


Figure 4 Mean reflectance spectra of 10 samples each with black spot, normal and different diseases over the wavelength range between 483 nm and 959 nm

All the spectral plots feature a local minimum around 675 nm. CBS and other conditions have the difference of local minimum due to light absorption of chlorophyll and carotenoid. As shown in Figure 4, the spectra from market fruit had the highest slope in reflectance vs. wavelengths from 500 nm to 575 nm, while other disorders increased at a lower rate in reflectance in this region. CBS remained fairly flat in this region, having a consistently lower reflectance than the other conditions. The spectral reflectance values of other disorders generally are bounded between the spectra of CBS (lowest) and market (highest) for wavelengths between 550 to 650 nm with reflectance ranging between 12% and 50%. In the region from 700 nm to 800 nm, the reflectance ranges between 40% and 70%. Reflectance spectra from hyperspectral images were extracted using ENVI 4.3 (ITT Visual Information Solutions, Boulder, CO).

#### 3.2 SID and SAM based classification

SID and SAM mappings were generated using the end spectra of CBS with the resulting rule images showing enhanced CBS regions. The SAM angle and SID divergence values of CBS ranged from 0.01 to about 0.1. Based on these values, a threshold algorithm was used to generate the binary classification image, which separated

CBS from other conditions by setting each pixel to either “1” for CBS or “0” for the other classes.

SID-based CBS classification results are shown in Table 1 for seven different threshold values. Classification trials were conducted by incrementally increasing the SID threshold value from the lowest value of 0.01 to the highest value of 0.07 at a step increment size of 0.01. As indicated in Table 2, the value of 0.04 provided the best overall performance of 97.14%. When the threshold was changed from 0.01 to 0.04, the classification accuracy increased from 74.28% to 97.14%, respectively. However, the overall classification accuracy peaked at threshold value 0.04 and decreased as the threshold value was further increased to 0.05. Based on the results shown in Table 2, the SID classification accuracy for “CBS” class was 98%, while the accuracy for “No CBS” class was 96.92%. Only three CBS samples were misclassified at the threshold value of 0.04, while 12 non CBS class samples were misclassified (eight greasy spot and four wind scar samples). All melanose and market samples were correctly classified at a 0.04 SID threshold. Therefore decisions can be made to optimize for CBS detection, rather than overall classification.

**Table 1 Misclassification for differentiating black spot from other conditions using SID mapping of hyperspectral images**

	Number	Threshold value						
		0.01	0.02	0.03	0.04	0.05	0.06	0.07
Black spot	135	135	66	12	3	2	2	0
Greasy spot	90	0	1	3	8	22	38	53
Market	90	0	0	0	0	1	1	1
Melanose	105	0	0	0	0	0	0	1
Wind scar	105	0	0	1	4	11	19	33
Accuracy/%		74.28	87.24	96.95	97.14	93.14	88.57	83.24
Avg. Overall accuracy /%		88.65						

During the SAM classification trials, shown in Table 3, the SAM threshold values were changed from 0.06 to 0.11 by a 0.01 increment. % (0.09) at the peak, and then decreased to about 90%. SAM showed similar classification accuracy characteristics to that of SID, however SAM mapping had a higher overall accuracy in the tested range. As shown in Table 4, for the best classification result, the classification accuracies for ‘CBS’ class, and ‘No CBS’ class were 98% and 97.95%,

respectively. There were three misclassified samples for ‘CBS’ class, and eight misclassified samples for ‘Non CBS’ class which consisted of greasy spot samples alone. The other three non-CBS classes (‘Market’, ‘Wind Scar’, and ‘Melanose’) had perfect classification results (100%). The plot of reflectance spectra in Figure 4 illustrated that greasy spot was very close to those of CBS, which contributed to the misclassification. Imaging parameters that will enhance the difference between the CBS samples and other confounding conditions such as greasy spot will be investigated in future studies. These will include looking into the effect of varying the illuminating source and changing the optical device to improve both reflectance and resolution of the images.

**Table 3 Misclassification for differentiating black spot from other conditions using SAM mapping of hyperspectral images**

	Number	Threshold value						
		0.06	0.07	0.08	0.09	0.10	0.11	0.12
Black spot	135	92	42	14	3	1	1	1
Greasy spot	90	0	0	2	8	16	29	44
Market	90	0	0	0	0	0	0	1
Melanose	105	0	0	0	0	0	0	0
Wind scar	105	0	0	0	0	2	4	6
Accuracy /%	525	82.48	92.00	96.95	97.90	96.38	93.52	90.10
Avg. Overall accuracy /%		92.76						

## 4 Discussion

In this study, a hyperspectral imaging system was developed to distinguish citrus fruits exhibiting symptoms of citrus black spot (CBS) from fruits with other peel conditions. Five fruit classes were evaluated; 1) CBS, 2) greasy spot, 3) melanose, 4) wind scar, and 5) market. The fruit samples were collected from a grove near Ft. Pierce, FL and hyperspectral images were collected at the University of Florida laboratory over a spectral range of 400 nm to 900 nm. Reference spectrum of CBS was obtained from the ROIs that were manually selected from the CBS hyperspectral images.

Based on the results, a CBS classification accuracy of 97.9% was obtained using the SAM approach with an optimal threshold value of 0.09. The SID mapping had a CBS classification accuracy of 97.14% with a 0.04 optimal threshold. All melanose and market fruit samples were correctly classified using the two mapping

approaches, while the accuracy for greasy spot was about 91% and wind scar was over 96%. Overall, the performances of both classification approaches in detecting CBS along with other peel conditions were very good. However, it was found that SAM was superior to SID in threshold sensitivity. SID's performance deteriorated faster as the threshold value moves away from the optimal threshold value, while SAM's classification performance was not greatly affected as the threshold was changed.

## 5 Conclusions

A large number of spectral channels in a hyperspectral images increase the potential of discriminating peel conditions between CBS and others. However, it presents challenges to image analysis because of the huge volume of data that the hyperspectral image usually consists of. Therefore, the appropriate hyperspectral mapping method is needed for further improvement of the classification accuracies.

This research demonstrated that hyperspectral imaging combined with an appropriate image processing algorithm such as SAM and SID mapping could be used for detecting CBS. The two hyperspectral image classification methodologies succeed in taking advantage of the spectral information for detecting CBS. The method performs well for images representing different conditions: those containing image data with spectrally confusing disease conditions and containing small and complex structures. Although this approach may not be appropriate for packinghouse applications, it demonstrates the potential for hyperspectral imaging to be used for identifying CBS among other confounding peel conditions.

Future studies will explore the identification of significant wavelengths from the reference spectrum to develop a multispectral imaging approach that could be applied in real time on packing line applications.

## [References]

- [1] Chung K R, Peres N A, Timmer L W. Citrus disease exotic to Florida: Black spot, Available from: [http://http://edis.ifas.ufl.edu](http://edis.ifas.ufl.edu). Accessed on [2011-03-01,]
- [2] Dewdney M M. 2010. Citrus black spot. *Citrus Ind.* 2010; 91: 19–20.
- [3] Dewdney M M, Yates J D, Ritenour M A. Identification of early citrus black spot symptoms (Identificación de los Síntomas Iniciales de la Mancha Negra de los Cítricos). Available from: <http://edis.ifas.ufl.edu/pp285>. Accessed on [2011-07-01].
- [4] Jimenez A R, Ceres R, Pons J L. A survey of computer vision methods for locating fruit on trees. *Transactions of the ASABE.* 2010; 43: 1911–1920.
- [5] Requinathan M, Lee W S. Citrus fruit identification and size determination using machine vision and ultrasonic sensors. paper no. 053017. In: ASAE Annual International Meeting. 17 July, Tampa Convention Center, Tampa, Florida, USA. American Society of Agricultural Engineers, Tampa, USA, 2005.
- [6] Burks T F, Shearer S A, Payne F A. Classification of weed species using color texture features and discriminant analysis. *Transactions of the ASAE,* 2000; 43: 441–448.
- [7] Tang L, Tian L F, Steward B L. Classification of broadleaf and grass weeds and an artificial neural network. *Transactions of the ASAE,* 2003; 46: 1247–1254.
- [8] Pydipati R, Bu Tang rks T F, Lee W S. Identification of citrus disease using color texture features and discriminant analysis. *Comput. Electron. Agr.,* 2006; 52: 49–59.
- [9] Du C J, Sun D W. Correlating image texture features extracted by five different methods with the tenderness of cooked pork ham: a feasibility study. *Transactions of the ASAE,* 2006; 49: 441–448.
- [10] Sun D W. *Hyperspectral imaging for food quality analysis and control.* Academic Press, Elsevier, San Diego, USA, 2006.
- [11] Jiang L, Zhu B, Rao X, Berney G, Tao Y. Discrimination of black walnut shell and pulp in hyper spectral fluorescence imagery using Gaussian kernel function approach. *J. Food Eng.,* 2007; 81: 108–117.
- [12] Zhang Y, He X J, Han J H. Texture feature-based image classification using wavelet package transform. *Advances in Intelligent Computing,* 2005; 3644: 165–173.
- [13] Kim M S, Chen Y R, Mehl P M. Hyperspectral reflectance and fluorescence imaging system for food quality and safety. *Transactions of the ASAE,* 2001; 44: 721–729.
- [14] Lee K J, Kang S, Kim M S, Noh S H. Hyper-spectral imaging for detection defect on apple. paper no. 053075. In: ASAE Annual International Meeting. 17 July, Tampa Convention Center, Tampa, Florida, USA. American Society of Agricultural Engineers, Tampa, USA, 2005.
- [15] Park B, Windham W R, Lawrence K C, Smith D P. Contaminant classification of poultry hyperspectral imagery using a spectral angle mapper algorithm. *Biosyst. Eng.,*

- 2007; 96: 323–333.
- [16] Qin J, Burks T F, Ritenour M A, Bonn W G. Detection of citrus canker using hyperspectral reflectance imaging with spectral information divergence. *J. Food Eng.*, 2009; 93: 183–191.
- [17] Yang C, Everitt J H, Bradford J M. Yield estimation from hyperspectral imagery using spectral angle mapper (SAM). *Transactions of the ASABE*, 2008; 51: 729–737.
- [18] Shippert P. Introduction to hyperspectral image analysis. Available from <http://spacejournal.ohio.edu/pdf/shippert.pdf>. Accessed on [2011-07-15].
- [19] Du Y, Chang C I, Ren H, Chang C C, Jensen J O. New hyperspectral discrimination measure for spectral characterization. *Opt. Eng.*, 2004; 43: 1777–1788.
- [20] Chang C I. Spectral information divergence for hyperspectral image analysis. In: *International Geoscience and Remote Sensing Symposium*. 28 June, Congress Center, Hamburg, Germany. IEEE Publications, Hamburg, Germany, 1999; pp. 509–511.